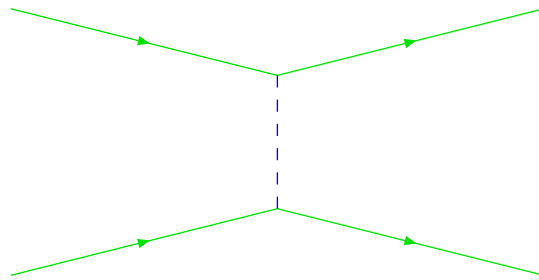


SLAC Experiment E158: A Precision Measurement of the Weak Mixing Angle in Møller Scattering

Michael Gary
Adviser: Yury Kolomensky

May 12, 2005



Abstract

Experiment E158 at the Stanford Linear Accelerator Center (SLAC) has measured, with unprecedented precision at low Q^2 , the parity non-conserving piece of the electroweak interaction governing Møller scattering ($e^- + e^- \rightarrow e^- + e^-$). Such a measurement of a right-left parity-violating asymmetry in Møller scattering allows one to test the functional dependence of the weak mixing angle on Q^2 . It also places limits on new physics beyond the Standard Model, such as existence of new electroweak bosons at TeV scales or electroweak compositeness at 10 TeV scales. The experiment, which consists of a 45 GeV or 48.3 GeV spin-polarized electron beam scattering off unpolarized electrons in a liquid Hydrogen target, has recently been completed and results are now being released.

Contents

1	Introduction	3
1.1	History	3
1.2	Motivation	3
1.3	Experimental Running	3
2	The Standard Model of Particle Physics	4
2.1	The Higgs Mechanism & Spontaneous Symmetry Breaking . .	6
2.2	Parity Violation in Electroweak Interactions	7
3	Møller Scattering	8
3.1	Parity Violating Asymmetry	8
4	Experimental Setup	10
4.1	Electron Beam	11
4.2	Target	13
4.3	Spectrometer	13
4.4	Beam Position Monitors	13
4.5	Calorimeter	14
4.6	Other Detectors	14
5	Data Analysis	14
5.1	First Order Errors	15
5.2	Higher Order Errors	16
5.2.1	Motivation for Second Order Analysis	16
5.2.2	Taylor Formalism	16
5.2.3	Error Estimates	17
5.2.4	Implementation	18
5.2.5	Results of Second Order Analysis	18
5.2.6	Work Remaining in Second Order Analysis	20
5.2.7	Conclusions from Second Order Analysis	21
6	Results	21
6.1	Parity Violating Asymmetry	21
6.2	Weak Mixing Angle	22
6.3	New Physics Limits	23
7	Acknowledgments	24

1 Introduction

1.1 History

About 50 years ago, the Russian physicist Yakov Zel'dovich predicted parity violating processes in electroweak neutral current interactions [1]. However, he immediately discounted any possibility of experimentally measuring this effect because he believed it to be too small, on the order of a few parts per billion. In 1978, spectacular demonstrations of parity violations were done in electron-deuteron scatterings at SLAC [2] and in atomic systems at Novosibirsk [3] and at Berkeley [4], leading to the establishment of Glashow-Weinberg-Salam model as the Standard Model of electroweak interactions (for which the three gentlemen received the Nobel Prize in 1979)[5]. While most measurements of electroweak parity violation occur at or near the Z^0 pole, recently experiments have begun to use precision measurements to determine the weak mixing angle away from the Z^0 pole.

1.2 Motivation

In the Glashow-Weinberg-Salam model of Electroweak theory, $\sin^2 \theta_W^{eff}$ is the ratio of the electromagnetic to weak isospin coupling constants. The value of $\sin^2 \theta_W^{eff}$ at $Q^2 \ll M_Z^2$ can be sensitive to new physics effects beyond the Standard Model at sensitivities comparable to high energy collider measurements, such as at LEP. At 1% precision, such as in E158, experiments are sensitive to the running of coupling constants, where the coupling varies with momentum transfer. While the electromagnetic and strong coupling constants have been observed to run, before E158, the running of $\sin^2 \theta_W^{eff}$ had not been unambiguously observed. The variation in coupling between $Q^2 \approx M_Z^2$ and $Q^2 \approx 0$ is due to loop level corrections involving virtual weak vector bosons and fermions, called radiative corrections (see Figure 6) [6, 7]. Prior to E158, most low energy experiments measuring the weak mixing angle were due to measurements of parity violation in atomic and neutrino-nucleon systems. However, E158 measures parity violation in Møller scattering, a purely leptonic process with little theoretical uncertainty, allowing for a more precise measurement.

1.3 Experimental Running

E158 ran in End Station A at SLAC with beam energies of 45 and 48.3 GeV at a rate of 120 Hz. The experiment consisted of a total of three physics runs, two runs in 2002 and one run in 2003 for a total of 2.9×10^8

45 GeV beam pulses and 3.7×10^8 48.3 GeV beam pulses. In addition to the physics runs, there were commissioning runs, both with a Carbon target and with the liquid Hydrogen target used in the experiment itself. During the experimental running, collaborators took turns working 8 hour shifts in pairs monitoring the experiment from the Counting House situated on top of End Station A, allowing the experiment to continue running continuously. During these shifts boredom often occurred, resulting in creation of works of art such as shown in Figure 1. However, shifts were not always boring, as exemplified by the shift during which a squirrel wandered into the SLAC power supply, causing a power surge followed by a brief power outage. This shutoff resulted in a small amount of Hydrogen being leaked from the target, setting off the Hydrogen alarm and summoning the SLAC fire department. In addition, upon restarting the circulation of the Hydrogen within the target, some liquid Hydrogen was splashed against a warm surface, causing rapid boiling and bursting a disk, leading to the venting of the entire target, which meant the experiment was shut down for several days while the target was repaired and refilled.

2 The Standard Model of Particle Physics

The Standard Model of particle physics attempts to describe the phenomena observed at accelerators and elsewhere in terms of fundamental particles and interactions with the intent of unifying the Electromagnetic, Strong, and Weak forces in one consistent theory. The Standard Model is a gauge theory described by a $U(1) \otimes SU(2) \otimes SU(3)$ local gauge group. The fundamental particles of the Standard Model can be divided into two classes, the fermions and the bosons. Once this subdivision has been made, the fermions can be divided into two classes, the leptons and the quarks. The left-handed leptons (see Figure 2) come in three “generations,” which are the electron and electron-neutrino, the muon and the muon-neutrino, and the tau and the tau-neutrino, where the neutrinos are electrically neutral and the electron, muon, and tau are all charged. The three generations of left-handed quarks are up and down, strange and charmed, and top and bottom, all electrically charged and coming in three “colors”. It should be noted that the Standard Model does not explain the three generations, nor does it associate the lepton generations with the quark generations. Along with all the left-handed particles are also their associated right-handed particles, which do not come in generations, as well as the associated anti-particles, which are

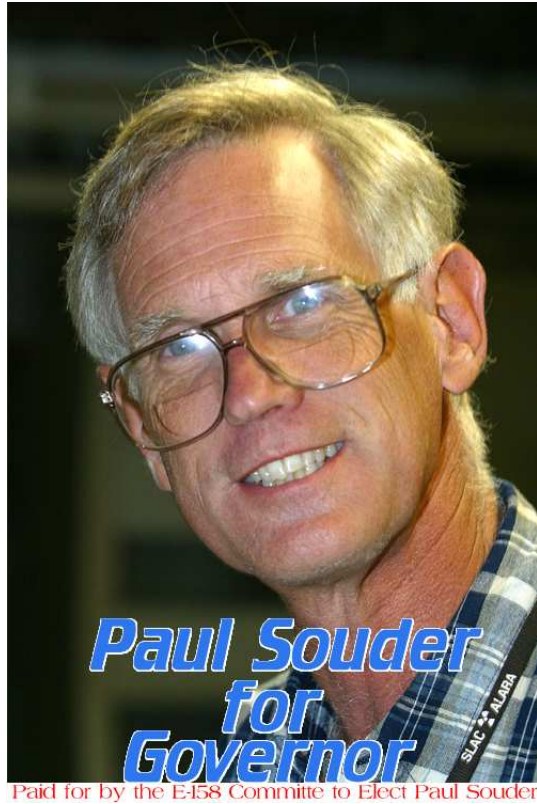


Figure 1: A result of boredom while working on shift

the Charge-Parity (CP) mirrors of the particles¹. In addition to the fermions, there are the bosons, which are associated with the gauge groups and mediate the forces associated with each symmetry. The $U(1)$ gauge symmetry describes the force associated with weak hyper-charge and gives rise to the boson B , mediating this force. The weak force is described by the $SU(2)$ isospin gauge symmetry, which gives rise to a vector triplet of three bosons, the W^0 , W^+ , and W^- , which mediate the force between the three generations of left-handed fermions. Finally, the strong force is described by the $SU(3)$ gauge symmetry, the so called “color” symmetry, and is mediated by bosons

¹Neutrinos are not well understood in the Standard Model. Until recently, they were believed to be massless, meaning that only the left-handed neutrino and right-handed anti-neutrino would exist. However, the recent observation of neutrino mass has invalidated this theory. One possible theory suggests that the neutrino is its own anti-particle, which would mean that the right-handed neutrino is the anti-neutrino. While experiments are underway to test this, such as those looking for neutrino-less double beta decay, to date no experimental evidence of this exists.

known as gluons, as described by Quantum ChromoDynamics. We will be most interested in the $U(1) \otimes SU(2)$ portion of the theory which describes the Glashow-Weinberg-Salam model of the electroweak force, since this is the primary portion of the Standard Model which is probed by E158.

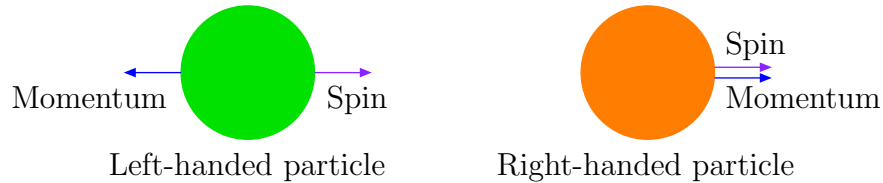


Figure 2: Left-handed particles have momentum oriented in the opposite direction from spin, while right-handed particles have momentum oriented in the same direction as spin.

2.1 The Higgs Mechanism & Spontaneous Symmetry Breaking

To understand spontaneous symmetry breaking, we will study a simple setup in which we break a global $U(1)$ gauge symmetry. While Electroweak symmetry breaking, the case in which we are interested, involves breaking a more complicated local gauge symmetry, this will give us a flavor for symmetry breaking. Consider an axially symmetric rod constrained to have its ends lie along its axis of symmetry (see Figure 3). Now allow the rod to be subjected to a compressive force along the axis of symmetry. Above a certain critical value of the force, the rod will no longer be able to sustain its straight position and will bend, breaking the axial symmetry (see Figure 4). However, there is no preferred direction in which the bend should occur, so there remains the freedom to choose which element of $U(1)$ describes the symmetry-broken ground state, although once this element has been fixed, the symmetry no longer applies. Also, with this broken symmetry comes a new massless boson that corresponds to rotating the rod about its former axis of symmetry (the boson is massless because the rotation can occur at any frequency, whereas a massive particle would require a minimum energy to go into mass, thus introducing a lower-energy cutoff). This new particle occurs generally when a global gauge symmetry is broken and is known as a Goldstone boson.

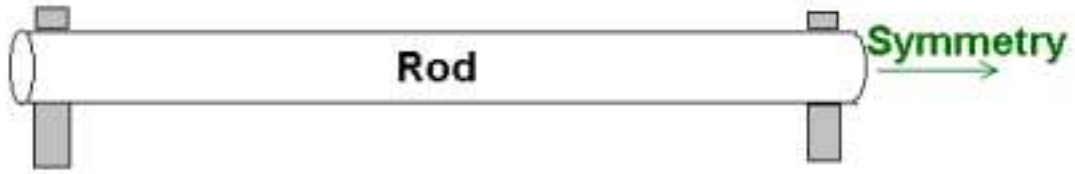


Figure 3: Unbroken Symmetry



Figure 4: Broken Symmetry

In the case of the Standard Model, the $U(1)_Y \otimes SU(2)_I$ local gauge symmetry is broken, which gives rise to a massive boson rather than the massless boson of a global gauge symmetry, known as a Higgs particle. In the process of breaking the gauge symmetry, the Higgs mechanism also gives mass to many of the particles. However, the mass eigenstates do not necessarily correspond to the eigenstates of the symmetries, such as the color eigenstate. Additionally, the Higgs field has a non-zero vacuum expectation value, meaning the probability of finding a Higgs particle at any given location is non-zero. The Higgs particle has not yet been observed, but many physicists believe it does exist and will be found and numerous experiments are underway searching for evidence of the Higgs particle.

2.2 Parity Violation in Electroweak Interactions

While the $U(1)_Y \otimes SU(2)_I$ gauge group is broken, a $U(1)_{EM}$ symmetry remains, generated by the linear combination $\frac{Y}{2} + I_3$, where Y is the generator of $U(1)_Y$ and I_3 is one of the generators of $SU(2)_I$. In effect, the Higgs mechanism “rotated” the B and the W^0 through an angle θ_W , the weak mixing angle, to form the new mass eigenstates γ and Z^0 . The γ remains massless, while the Z^0 is given a mass of about 92 GeV. The γ is also the generator of the $U(1)_{EM}$ symmetry and couples equally to left and right-handed charged fermions. The Z^0 , on the other hand, couples more strongly to left-handed

fermions than to right-handed fermions. However, both of these bosons are involved in mediating interactions between charged fermions. Therefore, the scattering cross section for left-handed particles differs from that of right-handed particles, which violates parity. To make this parity violating effect clear, note that the parity operator leaves axial quantities unchanged while inverting vector quantities, such as the Z^0 , so in a parity reversed universe, the Z^0 couples more strongly to the opposite handedness as in the original universe. It is this parity violating effect which E158 seeks to measure. Measuring the magnitude of the parity violation determines the value of the weak mixing angle.

3 Møller Scattering

In E158, spin-polarized electrons are scattered off unpolarized electrons in a process known as Møller scattering. Changing the polarization of the electrons in this process is equivalent to performing a parity operation, so measuring the difference between the scattering cross sections in the two helicities determines the magnitude of the parity violation in the electroweak interaction. Because we are scattering charged particles, either a γ or a Z^0 can be exchanged between the electrons, as shown in the tree level Feynman diagrams (Figure 5). We measure the interference between the parity conserving γ exchange and the parity violating Z^0 exchange.

While the tree level diagram displays the important properties we measure, it only takes into account effects up to first order in perturbation theory. Second order effects, characterized by loop level Feynman diagrams (Figure 6), can also contribute significantly to the asymmetry. In fact, taking these processes into account roughly halves the theoretically predicted parity violation. Fortunately, due to the small coupling constant of electroweak processes², terms higher than second order are suppressed and do not contribute significantly to the parity violation.

3.1 Parity Violating Asymmetry

Due to the low four-momentum transfer (Q^2) of E158, the primary scattering process observed is the parity conserving photon exchange. The differential cross section for this tree-level process is given by

²As opposed to the large coupling constant of QCD, which makes performing calculations difficult.

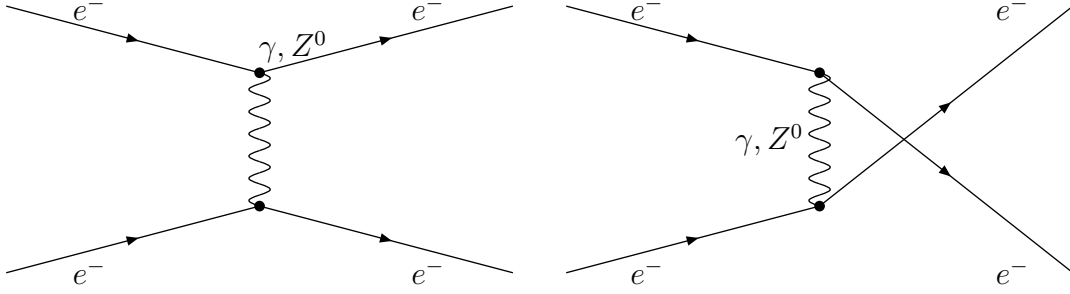


Figure 5: Møller Scattering Tree Level Feynman Diagrams

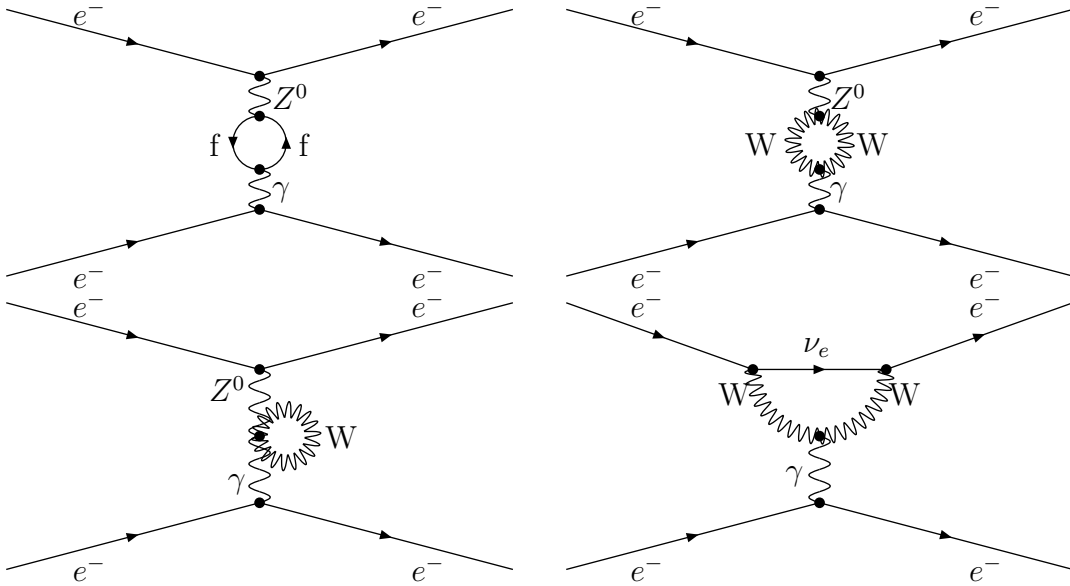


Figure 6: Møller Scattering Loop Level Feynman Diagrams

$$\frac{d\sigma}{d\Omega} = \frac{\alpha^2}{2mE} \frac{3 + \cos^2 \Theta}{\sin^4 \Theta} \quad (1)$$

where E is the incident beam energy, m is the electron mass, α is the fine structure constant, and Θ is the center of mass scattering angle. However, in actuality, two scattering processes occur: photon exchange and Z^0 exchange. While the photon exchange is dominant, the Z^0 exchange is not negligible at the precision level of $E158$. If we include both processes, then the scattering cross section contains a photon exchange term, a Z^0 exchange term, and an interference term. While the pure Z^0 exchange term is suppressed by a factor of G_F^2 and is therefore negligible, the interference term is proportional to $\frac{G_F}{\alpha}$, so it is not negligible. Additionally, the interference term is parity

violating, since it is proportional to an axial quantity times a vector quantity. Therefore, if we consider the parity violating asymmetry

$$A_{PV} = -A_{LR} = \frac{\sigma_R - \sigma_L}{\sigma_L + \sigma_R} \quad (2)$$

the quantity is non-zero and proportional to the interference term. Specifically, the parity violating asymmetry is given by the formula

$$A_{PV} = -mE \frac{G_F}{\sqrt{2}\pi\alpha} \frac{16 \sin^2 \Theta}{(3 + \cos^2 \Theta)} \left(\frac{1}{4} - \sin^2 \theta_W \right) \quad (3)$$

where θ_W is the weak mixing angle. Thus, by measuring the right-left asymmetry in Møller scattering, it is possible to measure the value of the weak mixing angle.

4 Experimental Setup

The fundamental idea of E158 is to measure the parity violating asymmetry in Møller scattering at $Q^2 \approx 0.03(GeV/c)^2$. In order to measure the interference term, we measure the scattering rate for pseudo-randomly generated pairs of left-right beam pulses then combine these results into a left-right asymmetry as defined above in formula 2. This asymmetry is then averaged over a large number of pairs in order to reduce the statistical error. In order for this method to be effective, the systematic effects due to differences in the beam properties between the left and right-handed beam pulses, helicity-correlated systematics, need to be minimized. If these effects were dominant, as illustrated in Figure 7, the parity violating asymmetry would be lost within the error. Therefore measuring and controlling such effects is one of the primary difficulties in performing such a measurement, and much of the effort in E158 goes into such details.

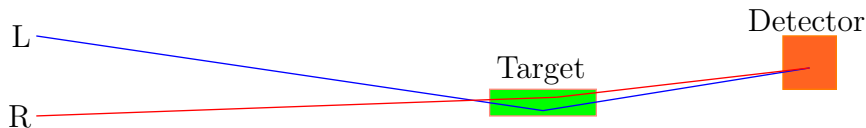


Figure 7: Differences between left and right-handed beam pulses, as shown, can lead to systematic errors because they induce a false asymmetry.

Before studying any individual experimental apparatus in detail, it is useful to get a general overview of the experimental setup. A spin-polarized

electron beam is generated and sent through the linear accelerator. Upon emerging from the accelerator, the beam properties are measured, then the beam scatters off unpolarized electrons in a liquid Hydrogen target. Dipole magnets are then used to steer the electrons around a collimator, while neutral particles are stopped by the collimators. Quadrupole magnets are then used to focus the Møller scattered electrons while defocusing the Mott ($e^- + p \rightarrow e^- + p$) scattered electrons. The electron energies are then measured by an integrating calorimeter constructed from copper and fused silica. This setup can be summarized by the schematics seen in Figures 8 and 9, which show the beam-line as a whole and End Station A—where the target, detector, and magnets reside—respectively.

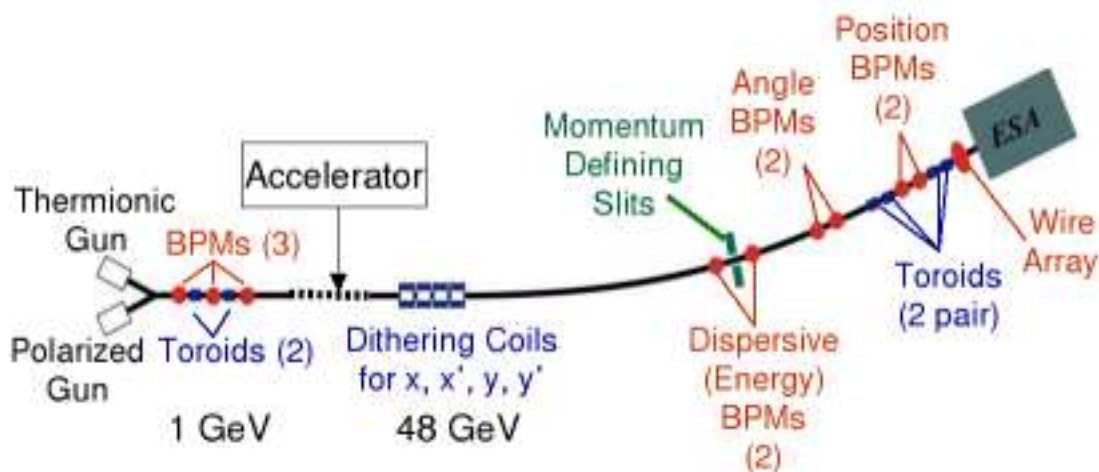


Figure 8: E158 Beam-line

4.1 Electron Beam

E158 requires a polarized electron beam, which is achieved by photo-emission from a strained GaAs cathode. Specifically, a flash-lamp pumped Ti:Sapphire laser produces coherent light, which is then passed through a linear polarizer, followed by two Pockels cells, which produce either left-handed or right-handed circularly polarized light depending on the voltages applied across their faces. This allows the rapid pseudo-random alternation of left-handed and right-handed beam pulses. Additionally, feedback based on measurements of the beam taken slightly down-line is used to adjust the applied voltages to reduce systematic helicity correlated effects due to variations in

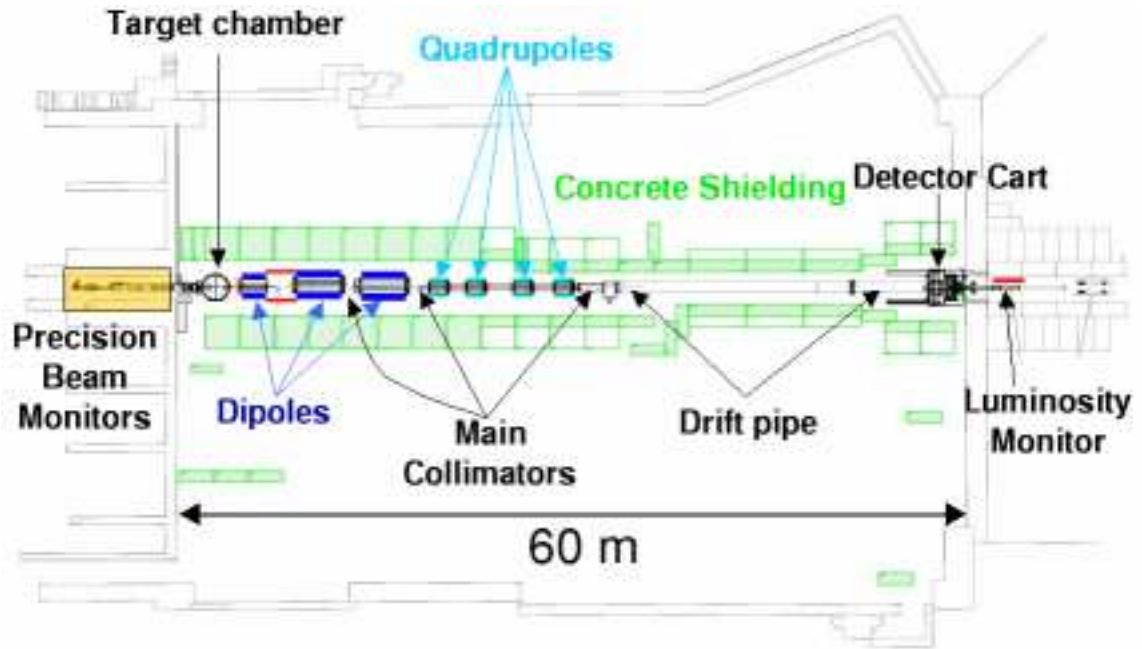


Figure 9: End Station A Setup

the laser. This is necessary, since many of the beam properties, such as charge within a beam pulse, are associated with the properties of the laser light used to generate the beam. The laser pulse lasts approximately 200 to 350 ns and produces beam pulses with between 3×10^{11} and 6×10^{11} electrons. This process is repeated at 120 Hz with pseudo-random alternation of left and right-handed beam pulses. Also, a half-wave-plate is inserted and removed from the optics on an approximately daily basis, reversing the role of the Pockels cells in an attempt to further reduce any helicity correlated effects. Furthermore, the beam energy alternates between 45 GeV and 48.3 GeV throughout running, which changes the number of $g - 2$ precessions between the beam-line and the End Station by 1/2, which reverses the role of left and right-handed laser pulses again. Thus, the electron beam is carefully controlled in an attempt to reduce systematic effects. However, controlling the beam alone is not enough to make helicity correlated systematic effects small so other methods are also used to help control these effects, as will be discussed later.

4.2 Target

In E158, we scatter polarized electrons off unpolarized atomic electrons in a Liquid Hydrogen target. Liquid Hydrogen has the shortest radiation length per target electron, making it a very practical target choice. Additionally, the Mott ($e^- + p \rightarrow e^- + p$) scattering cross section and asymmetry is smallest for Hydrogen, which means the background is smaller. The target itself consists of a cylindrical tank of liquid Hydrogen approximately 3 inches in diameter and 150 centimeters in length. The Hydrogen is circulated through the system and is maintained at 20 Kelvin via a heat exchanger. While this system works well, should the Hydrogen start to solidify, the impeller motor would likely break, taking our target offline for a significant length of time. Therefore, care needs to be taken to ensure this does not happen. Also, if the impeller splashes a cold liquid on a warm surface, such as happened during Run III, the liquid will boil, causing a disk to burst and the target to vent, taking the experiment offline for several days.

4.3 Spectrometer

The spectrometer is designed to separate the Møller and Mott electrons as well as to remove the bremsstrahlung background. Scattered Møller electrons with energies between 12 GeV and 24 GeV, corresponding to center of mass scattering angles with $-0.5 < \cos\theta < 0$, are passed by the spectrometer. The spectrometer itself consists of three dipole magnets, which bend the charged particles around a collimator which blocks the neutral particles, and four quadrupole magnets, which focus the Møller scattered electrons while defocusing the more energetic Mott scattered electrons to the outer regions of the calorimeter.

4.4 Beam Position Monitors

To control systematic effects due to asymmetries between the left and right handed beam pulses, it is important that we measure these differences. To this ends, there are a large number of precision beam position monitors (BPMs) and toroids installed along the beamline. Beam position monitors consist of resonant cavities which are used to measure beam parameters while the toroids are used to measure the beam charge. Specifically, the BPMs come in units, which consist of three BPMs, one to measure charge and two to measure position, one for measuring X and one for measuring Y. In combination, two units can be used to measure the angle of the beam as well, along with providing a consistency check between the two units. Also, BPMs

located along the bend in the accelerator can be used to measure the beam energy. In total, the BPMs measure the beam parameters Q , X , Y , dX , dY , and E , while the toroids measure Q . There are two toroids located near the beam source and four toroids located in the alcove just before the target. There are three BPM units placed near the beam source, five units placed along the A-line, where the beam travels to reach End Station A, and two more units placed in the alcove before the target.

4.5 Calorimeter

The Copper and fused Silica calorimeter is the primary detector used in E158. High energy electrons entering the calorimeter produce high energy photons by bremsstrahlung. These photons then pair produce into electron-positron pairs, which repeat the bremsstrahlung process. This process continues in the copper, producing a shower of relativistic charged particles. These charged particles then pass through the fused silica bands within the copper, producing Cerenkov radiation, which travels through the fused silica into photomultiplier tubes. Via this process, the total energy deposited within any detector region can be measured. The detector is divided into three rings, each of which are divided into regions. By dividing each of the rings into sections, possible azimuthally dependent effects can be measured. The Mott background is measured by the same process in the outer rings to determine the background.

4.6 Other Detectors

In addition to the above described detectors, there is a detector which measures the beam luminosity, a calorimeter which measures the forward angle Mott energy, pion and muon detector to determine the pion and muon backgrounds, and a Cerenkov counter to measure the amount of Cerenkov radiation produced.

5 Data Analysis

While in the ideal case, the electron beam would be identical between left and right-handed pulses, this is not possible. Differences between beam pulses have been reduced as much as possible, but some differences remain, as shown in Figure 7. Therefore, we must take these differences into account and attempt to remove these false asymmetries from the measurement. This is done by measuring a set of parameters which are believed to fully describe the

beam, then removing any asymmetries associated with differences in these parameters between left and right-handed beam pulses.

5.1 First Order Errors

The beam is believed to be described fully by its charge, energy, position, and angle, which are labeled Q, E, X, Y, dX, and dY, respectively, where X and Y are position variables and dX and dY are angle variables. These beam parameters are measured for each beam pulse and the asymmetry is regressed against any differences in these beam parameters between the left and right-handed beam pulses. More concretely, the asymmetry is given by $A_{meas} = A_{phys} - \sum_i \alpha_i \Delta X_i$, where A is an asymmetry, i runs over the beam parameters, ΔX_i is the asymmetry in beam parameter i , and α_i is the correlation between a parameter asymmetry and the measured asymmetry (up to a sign for convenience), referred to as a detector slope. The values of the α_i are determined by a least squares fit linear regression and thus are subject to an error due to the uncertainty in the least squares fit. This modifies the formula for the physical asymmetry to

$$A_{phys} = A_{meas} + \sum_i \alpha_i \Delta X_i + \epsilon_i \quad (4)$$

where ϵ_i is the error due to the uncertainty in the fit of α_i . [8]

During Runs I and II of E158, we did not actually measure the values of ΔX_i , but rather, we measured the values of $\Delta \langle X_i \rangle$, where $\langle \rangle$ denotes a time average taken over a beam pulse. Therefore, the asymmetry determined by the matrix regression is actually

$$A_{reg} = A_{meas} + \sum_i \langle \alpha_i \rangle \Delta \langle X_i \rangle + \langle \epsilon_i \rangle. \quad (5)$$

While to first order, A_{reg} is the same as A_{phys} , if the values of ΔX_i and α_i vary within beam pulses, A_{phys} is no longer equal to A_{reg} . Specifically, if α_i depends on the value of X_i and X_i varies within a beam pulse, there can be large differences between A_{phys} and A_{reg} . These effects were assumed to be negligible when the experiment was designed. However, during data analysis, it became clear that this was not the case, so Beam Position Monitors capable of resolving time dependent effects, so called time slice BPMs, were installed during Run III, allowing the presence of such effects to be confirmed. Because no such data exists for Runs I and II, a method of estimating the error due to the assumptions is needed.

5.2 Higher Order Errors

In this section, I provide a description of the computerized Taylor analysis of the second order E-158 beam systematics. The purpose of the Taylor analysis is to determine the effects of non-linear beam shapes on observed false asymmetries. In essence, the idea is to feed various beam shapes and detector responses into a program and obtain predictions for the observed false asymmetries. Based on these predictions, we hope to be able to estimate the systematic errors due to non-linear effects.

5.2.1 Motivation for Second Order Analysis

It has become clear throughout the course of data analysis that the linear regression is not accounting for all systematic effects in the asymmetry [10]. Specifically, in Runs I and II, the OUT asymmetries showed large (relative to statistics) fluctuations inconsistent with first order effects in the six beam parameters. In Run III, slice signals were added to BPMs to measure asymmetry as a function of time within individual beam pulses. Regressing against these additional signals corrects many of the problems found in the OUT monopoles. This dependence is a strong indicator that the large χ^2 values measured in Runs I and II are due to time dependent beam effects. Such effects appear in the differences between coherent and decoherent time averages of second order terms in the Taylor expansion of the cross section, which has lead such effects to be called second order effects. By understanding the origins and sizes of second order effects, we hope to place a meaningful limit on the size of the systematic errors due to second order effects in Runs I and II. Specifically, we hope to estimate the ratio of the second order effects in INs and MIDs to OUTs in all three runs in order to place limits on the systematic errors due to second order effects in Runs I and II in the INs and MIDs based on the size of the OUTs in each run, respectively.

5.2.2 Taylor Formalism

It is typically assumed that dependence of a given detector channel's signal d_i on each of the beam parameters is approximately linear over the range of the beam jitter, yielding the formula for measured asymmetry in detector i , A_i :

$$A_i = \frac{d_{iR} - d_{iL}}{d_{iR} + d_{iL}} = A_i^{phys} + \sum_k \alpha_{ki} \Delta X_k \quad (6)$$

where k runs over all beam parameters and $\alpha_{ki} = \frac{\partial A_i}{\partial X_k}$ is the detector slope, and ΔX_k is the asymmetry in parameter k [9]. However, in light of the

recent findings that the beam parameters are non-linear in time, making the detector response, which depends on the value of the beam parameter, non-linear and time dependent, with non-negligible effects up to second order, we are lead to a new formula for the measured asymmetry:

$$A_i = A_i^{phys} + \sum_k \alpha_{ki} \left(1 + \sum_\ell \beta_{\ell ki} X_\ell \right) \Delta X_k \quad (7)$$

where $\beta_{\ell ki} = \frac{1}{2\alpha_{ki}} \frac{\partial \alpha_{ki}}{\partial x_\ell}$. Additionally, we need to take a time average over a beam pulse of the asymmetry, since we actually measure the average asymmetry in a pulse. The fact that the measured asymmetry is a coherent time average while the data analysis assumes a decoherent time average leads to a false asymmetry, as shown in equation 8. The slice data collected during Run III seems to suggest this effect is non-negligible, which motivates us to perform an analysis of second order asymmetries.

$$A_{false} = A_{reg} - A_{phys} = \sum_i \langle \alpha_i \rangle \Delta \langle X_i \rangle - \langle \alpha_i \Delta X_i \rangle \quad (8)$$

5.2.3 Error Estimates

Because the slice data was not collected during Runs I and II, we are forced to estimate the systematic errors due to second order effects. One method for estimating the errors in INs and MIDs involves using the known errors in the OUTs from Runs I and II and estimated ratios of errors between the INs and OUTs and the MIDs and OUTs found using the Taylor formalism. In this method, the false beam asymmetry is given by the formula:

$$\delta_i = \alpha_i A_{syst} = \frac{(A_{OUT}^{phys} - A_i^{phys}) - (A_{OUT} - A_i)}{\frac{\alpha_{OUT}}{\alpha_i} - 1} \quad (9)$$

where i ranges over IN and MID, A^{phys} is the real physics asymmetry as predicted by theory, A is the (average) measured asymmetry, and α is the coupling to the detector asymmetry [10] (Note that while some variables in formula 9 look similar to those in formulas 6 and 7, they are in fact different). The difference in the theoretical physics asymmetries between detectors is due primarily to EP contributions, which differ between INs, MIDs, and OUTs. The only unknown in the above formula is the ratio of the detector couplings $\frac{\alpha_{OUT}}{\alpha_i}$, and it is this quantity we seek to estimate. If we can estimate the second order asymmetries for both OUT and detector i , then we know the ratio of the couplings, since it is simply the ratio of the second order asymmetries.

5.2.4 Implementation

Since the slice implementation during Run III only had four time slices of resolution, little is known about the possible beam shapes. Therefore, the ability to test the effects of a wide variety of beam shapes is desirable. Since the amount of computation required for an individual beam shape is not so insignificant as to be quickly done by hand, computing false asymmetries for a variety of beam shapes is a task best left to a computer. This leaves two reasonable options: write a program to compute directly the terms in the Taylor Series and the resulting second order effects, or program these second order effects into Peter Mastromarino’s Beam Monte Carlo. The advantages of the Beam Monte Carlo are that it is already mostly written and easily provides error estimates, while the advantages of the stand-alone code are that it is faster due to the fact that it is only designed to provide one result and that the code is simpler to understand. Initially, we attempted to modify the Beam Monte Carlo. While this method was successful in producing second order effects, doing so was time consuming, requiring at least four hours per beam shape considered since the Monte Carlo makes use of the full analysis used on the experimental data. Because of the slow progress of the Monte Carlo, we decided to write a stand-alone program to compute the effects instead. In order to maintain the ability to easily compare results to the modified beam Monte Carlo, both programs take the same format of input file and divide individual beam pulses into ten time slices, during each of which all of the beam parameters and asymmetries may take on independent values. While this discrete time slicing does not allow for all possible beam shapes, it provides greater resolution than was implemented in run 3 and allows for the suspected beam shapes, namely linear, quadratic, and “tail wagging,” in which parameter values differ wildly from the average during the final time slice. Also, based upon observations during running, it was assumed that most of the dominant effects are concentrated in the beam parameters E and X , although this assumption is not hard-coded into the program itself and is rather reflected in the choice of input files.

5.2.5 Results of Second Order Analysis

The program was run with 81 combinations of beam shapes and asymmetries with slopes from each of Runs I, II, and III. For Run I, the slopes were taken from those calculated for run 4835, for Run II from run 7103, and for Run III from run 9803, all three of which are randomly chosen and typical of the runs within their Run. The higher derivatives were calculated based on the result of Brock Tweed’s Monte Carlo simulation [11] and were assumed to

be independent of the Run. Full results can be found on line at <http://www.slac.stanford.edu/~mgary/toyMC.html>.

Assuming all beam shapes are equally likely, we find the average results given in tables 1, 2, and 3.

	IN	MID	OUT	OUT/IN	OUT/MID
Monopole	0.332	0.650	9.34	-30.5	15.4
dipole X	24.3	43.8	478.	-106.	9.64
dipole X	6.96	16.4	485.	53.4	20.2

Table 1: Run I Average Results

	IN	MID	OUT	OUT/IN	OUT/MID
Monopole	0.260	0.327	14.4	65.9	29.7
dipole X	18.9	22.7	599.	40.8	17.7
dipole X	5.44	7.56	811.	182.	74.5

Table 2: Run II Average Results

	IN	MID	OUT	OUT/IN	OUT/MID
Monopole	2.40	789.	1310	231.	1.49
dipole X	182.	43400	72800	2110	1.50
dipole X	25.7	33900	53800	1110	1.12

Table 3: Run III Average Results

It is interesting to note that the ratio of OUTs to MIDs in Run III (see table 3) is of order unity, as should be expected, since during Run III the Quads were set to make Møller contributions in the MIDs and OUTs roughly the same size. Also, the monopole ratios of OUTs to MIDs and INs are larger in Run II than in Run I as observed in the actual data.

Looking at the results from the computer analysis available on the website listed above, we notice that some beam shapes can produce large ratios of asymmetries (OUT/IN, OUT/MID), sometimes as much as an order of magnitude greater than the mean. However, large asymmetries contribute little to the estimate of the systematic error due to second order effects, and in fact excluding these large terms from the mean increases the error estimate

slightly. Thus, including a cut for these large ratios is a more conservative estimate of the error. Using this more conservative cut, we find the average results given in tables 4, 5, and 6.

	IN	MID	OUT	OUT/IN	OUT/MID
Monopole	0.408	0.790	11.3	29.8	14.4
dipole X	29.8	52.7	580	20.5	10.6
dipole X	8.60	20.2	585.	80.5	32.6

Table 4: Run I Average Results With Cut

	IN	MID	OUT	OUT/IN	OUT/MID
Monopole	0.260	0.327	14.4	65.9	29.7
dipole X	18.9	22.7	599.	40.8	17.7
dipole X	5.44	7.56	811.	182.	74.5

Table 5: Run II Average Results With Cut

	IN	MID	OUT	OUT/IN	OUT/MID
Monopole	2.66	856.	1420	75.9	1.49
dipole X	202.	47000	79000	39.9	1.51
dipole X	29.8	36800	58400	1380	1.55

Table 6: Run III Average Results With Cut

We now turn our attention to estimating the systematic errors in Runs I and II due to the second order effects using the method given by Yury Kolomensky[10] (see formula 9). Since we have calculated the ratios of OUTs to INs and MIDs, we can simply plug these numbers into formula 9. Doing so yields results given in table 7.

5.2.6 Work Remaining in Second Order Analysis

The Taylor analysis code remains a work in progress. Currently, the code fails to provide output for unknown reasons when both delta X and delta E are quadratic in shape. Eventually, the intention is to compare the results of this analysis to the results of an independent MonteCarlo simulation of beam systematics originally programmed by Peter Mastromarino [12] which

Run	Error Without Cuts (ppb)	Error With Cuts (ppb)
I	6.8	7.3
II	2.4	3.1

Table 7: Systematic Errors Due to Second Order Effects

was updated to allow for non-linear detector response and time-dependent beam parameters. While comparisons have already been made for a few beam shapes, comparing results for all 81 tested beam shapes for all three runs will take a significant time commitment.

5.2.7 Conclusions from Second Order Analysis

We provided a method for estimating the systematic errors due to higher order effects and estimated this error in Runs I and II. We find numbers around 7 ppb for Run I and 3 ppb for run II. These numbers are consistent with the other estimates provided by Yury [10].

6 Results

6.1 Parity Violating Asymmetry

In addition to the false asymmetries described in section 5, the physical asymmetry is also corrected for background contributions (such as the background due to Mott scattering), detector linearity, and beam polarization. With the corrections taken into account, the physical asymmetry A_{phys} is given by

$$A_{phys} = \frac{1}{P_b \epsilon} \frac{A_{raw} - \sum_i \Delta A_i}{1 - \sum_i f_i} \quad (10)$$

where A_i are false asymmetries, f_i are dilution factors from various sources as listed in table 8, P_b is the beam polarization, measured to be 0.89 ± 0.04 , and ϵ is the calorimeter linearity, determined to be 0.99 ± 0.01 during calibration runs. The raw asymmetry A_{raw} has an RMS of 215 ppm for Runs I and II and an RMS of 185 ppm for Run III. The combined result is

$$A_{PV} = -131 \pm 14(stat.) \pm 10(syst.)ppb. \quad (11)$$

Source	ΔA (ppb)	f
Beam (first order)	-10 ± 1	
Beam (higher order)	0 ± 3	
Transverse polarization	-4 ± 2	
$e^- + p \rightarrow e^- + p(+\gamma)$	-7 ± 1	0.056 ± 0.007
$e^-(+\gamma) + p \rightarrow e^- + X$	-22 ± 4	0.009 ± 0.001
$\gamma + e^- \rightarrow e^- + \gamma$	0 ± 1	0.005 ± 0.002
High energy photons	3 ± 4	0.004 ± 0.002
Synchrotron photons	0 ± 1	0.002 ± 0.001
Pions	1 ± 1	0.001 ± 0.001

Table 8: Corrections ΔA_i and dilutions f_i to A_{raw} and associated systematic uncertainties.[13]

6.2 Weak Mixing Angle

As described in section 2.2, the measured value of A_{PV} can be used to determine the effective value of the weak mixing angle at a particular value of Q^2 , the four-momentum transfer, and s , the square of the center-of-mass energy.

$$A_{PV} = -\mathcal{A}(Q^2, y)\rho^{(e;e)} \left(1 - 4 \sin^2 \theta_W^{eff}(Q) + \Delta\right) \quad (12)$$

The average value of Q^2 is $0.026 GeV^2$ and the average value of $y = Q^2/s \approx 0.6$.

$$\mathcal{A}(Q^2, y) = \frac{G_F Q^2}{\sqrt{2}\pi\alpha(Q)} \frac{1-y}{1+y^4+(1-y)^4} \mathcal{F}_{QED} \quad (13)$$

is the effective analyzing power, G_F and $\alpha(Q)$ are the Fermi and fine structure constants, respectively, $\rho^{(e;e)}$ is the low-energy ratio of the weak neutral and charge current couplings, $\mathcal{F}_{QED} = 1.01 \pm 0.01$ is a QED radiative correction factor, and Δ contains $\mathcal{O}(\alpha)$ electroweak corrections. The effective analyzing power $\mathcal{A} = 3.25 \pm 0.05 ppm$ is determined from a Monte Carlo simulation. [13]

Adopting a definition of $\sin^2 \theta_W^{eff}(Q)$ which reproduces the effective leptonic coupling $\sin^2 \theta_W^{eff}(M_Z) = 0.23149 \pm 0.00015$ implies $\rho^{(e;e)} = 1.0012 \pm 0.0005$ and $\Delta = -0.0007 \pm 0.0009$, which determines

$$\sin^2 \theta_W^{eff}(Q) = 0.2397 \pm 0.0010(stat.) \pm 0.0008(syst.). \quad (14)$$

This value is consistent with the Standard Model and is 6.2σ from $\sin^2 \theta_W^{eff}(M_Z)$ (see Figure 10). If we evolve this result to the Z^0 pole, we find

$$\sin^2 \theta_W(M_Z)_{\bar{M}S} = 0.2330 \pm 0.0011(stat.) \pm 0.0009(syst.) \pm 0.0006(theory). \quad (15)$$

The theoretical uncertainty results from the evolution to the Z^0 pole. [13]

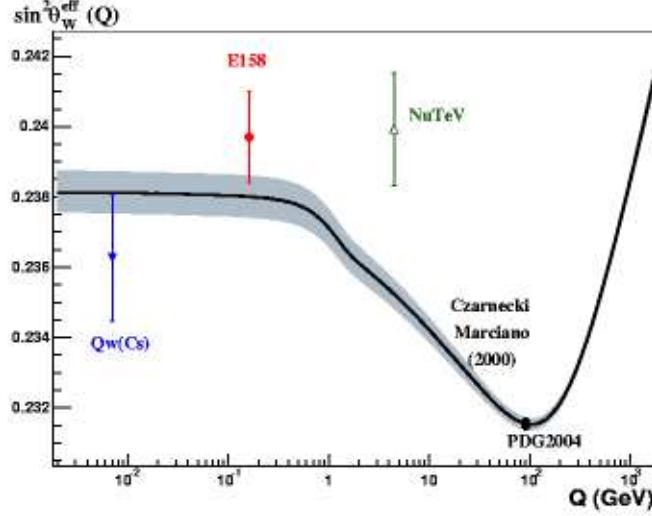


Figure 10: Predicted variation of $\sin^2 \theta_W^{eff}$ as a function of momentum transfer Q (solid line) and its estimated theoretical uncertainty (shaded area). Results of prior low energy experiments are shown together with the Z^0 pole value and the E158 measurement.[13]

6.3 New Physics Limits

Suppose a new interaction beyond the Standard Model were to exist. Since such an interaction has not been observed yet, so the particle mediating the interaction should have mass M far above the currently accessible scales. Therefore, any interaction involving such a particle at the energy of E158 would look like a contact interaction between the electrons. Such a left-handed contact interaction would be described by a term in the Lagrangian $\mathcal{L} = \pm(4\pi/2\Lambda_{LL}^{\pm})^2(\bar{e}_L\gamma_\mu e_L)$, where Λ_{LL}^{\pm} is the mass of the new particle. Based on the E158 data, at the 95% C.L. tree-level calculations set $\Lambda_{LL}^+ \geq 7TeV$ and $\Lambda_{LL}^- \geq 16TeV$ for potential positive and negative deviations, respectively. Specifically, the 95% C.L. on the mass of a Z_χ boson in a grand unified $SO(10)$ model is $M_Z \geq 1.0TeV$. [13]

7 Acknowledgments

First and foremost, I would like to thank Yury Kolomensky, for his willingness to take me on as an undergraduate student researcher, for his providing mentorship in the ideas of particle experiment, for his willingness to explain concepts to me multiple times, for his advising me, both in respect to courses at Berkeley and in respect to the graduate school application process, and for his insight into error estimation—which lead him to be likened to a natural wonder of the world by an anonymous collaborator. I would also like to thank Zach Marshall for his help in writing my first E158 technical note and for commiserating over frustrations with me. Additionally, I want to thank Brock Tweedie for his discussions of Monte Carlo simulation, theoretical physics, and super-symmetry. Finally, I wish to thank Mark Cooke for his explanations of the Standard Model of Particle Physics, Electroweak Symmetry Breaking, and the use of time slices in E158.

References

- [1] Ya.B. Zel'dovich. Sov. Phys. JEP **94**, 262 (1959).
- [2] C. Prescott et al. Phys. Lett. B **77**, 347 (1978).
- [3] L. M. Barkov and M. S. Zolotoryov. Pis'ma Zh. Eksp. Teor. Fiz. **27**, 379 (1978).
- [4] P. Bucksbaum, E. Commins, and L. Hunter. Phys. Rev. Lett. **46**, 640 (1981).
- [5] S.L. Glashow, J. Iliopoulos and L. Maiani. Phys. Rev. **D2**, 1285 (1970); A. Salam. *Elementary Particle Physics*, ed. N. Svartholm(Almqvist and Wiksell, Stockholm, 1968) p. 367; S. Weinberg. Phys. Rev. Lett. **19**, 1264 (1967).
- [6] A. Czarnecki and W.J. Marciano, Phys. Rev. **D53**, 1066 (1996).
- [7] J. Erler, A. Kurylov, and M.J. Ramsey-Musolf, Phys. Rev. **D53**, 016006 (2003); A. Rerrogia, G. Ossola, and A. Sirlin, Eur. Phys. J. **C34**, 165 (2004); J. Erler and M.J. Ramsey-Musolf, preprint hep-ph/0409169; F.J. Petriello, Phys. Rev. **D68**, 033006 (2003).
- [8] Zachary Marshall. Technical Note #51: "Regression Using Covariance Matrices in E-158".
- [9] Peter Mastromarino. "A Precision Low-Energy Measurement of the Weak Mixing Angle in Moller Scattering". <http://www.slac.stanford.edu/exp/e158/documents/theses/peterm-thesis.pdf>.
- [10] Yury Kolomensky. Technical Note #56: "Higher Order Asymmetry Systematics".

- [11] Brock Tweedie. Technical Note #37: “The GEANT3 Simulation of E-158”.

- [12] Peter Mastromarino. Technical Note #20: “Analysis of Beam Asymmetries for E-158 Commissioning Run”.

- [13] SLAC E158 Collaboration: P.L. Anthony et al. “Precision Measurement of the Weak Mixing Angle in Møller Scattering”. preprint hep-ex/0504049 (2005).